PHYSICAL REVIEW B **68**, 134444 (2003)

Strain-induced orbital ordering in thin $La_{0.7}Ca_{0.3}MnO_3$ films on $SrTiO_3$

M. Ziese,* H. C. Semmelhack, and K. H. Han
Division of Superconductivity and Magnetism, University of Leipzig, 04103 Leipzig, Germany

(Received 10 October 2002; revised manuscript received 19 June 2003; published 24 October 2003)

The microstructural, magnetic, and magnetotransport properties of $La_{0.7}Ca_{0.3}MnO_3$ films epitaxially grown on $SrTiO_3$ substrates were studied as a function of film thickness. Films with a thickness above 70 nm show bulklike properties consistent with the relaxed film growth. Very thin films are fully strained and are insulating and ferromagnetic in zero field. Under the application of a large magnetic field a strongly hysteretic metal-insulator transition is seen accompanied by a transition to a ferromagnetic state with larger saturation magnetization. The field-induced metallic state is shown to be anisotropic with metallic domains extending along the field direction. An analysis of the microstructure shows that the strain variation across growth islands is far too small to induce strain-related phase separation on length scales of the order of 100 nm. It is concluded that the insulating state is a property of homogeneously strained manganite films and arises from a weakening of the double-exchange interaction due to the ordering of atomic orbitals.

DOI: 10.1103/PhysRevB.68.134444 PACS number(s): 73.50.Jt, 75.47.Gk, 75.70.−i

I. INTRODUCTION

The colossal magnetoresistance (CMR) manganites of the type $La_{1-x}Ca_xMnO_3$ have attracted considerable experimental and theoretical interest, since these display a complex phase diagram due to the intricate interplay between charge, spin, and orbital degrees of freedom.[1] At an optimal doping $x=0.3$ the manganites crystallize in a pseudocubic structure with a ferromagnetic low-temperature state. In the cubic structure the e_g orbitals are energetically degenerate. If a uniaxial or biaxial distortion is applied, this degeneracy is lifted and an ordering of the $3z^2-r^2$ orbital along the uniaxial axis and of the x^2-y^2 orbital within the biaxial stress plane occurs. This has severe consequences on the relative magnitude of the ferromagnetic double-exchange and antiferromagnetic superexchange interactions and might lead to transitions from a ferromagnetic state in the undistorted material to *A*- or *C*-type antiferromagnetic states under uniaxial deformation.[2]

A route to study such effects experimentally is by the growth of coherently strained epitaxial films on various substrates.[3–11] The film-substrate mismatch leads to a biaxial distortion of the film and by this route c/a ratios of the tetragonal cell ranging from 0.97 to 1.06 can be achieved. In thin, presumably coherently strained films transitions from metallic to insulating behavior have been observed.[3,4,6] Whereas the metallic state is doubtless ferromagnetic, the magnetic nature of the insulating state is less clear. Here $Nd_{1-x}Sr_xMnO_3$ serves as a model system and in analogy with its phase diagram the insulating state in strained films has been suggested to be antiferromagnetic.[3]

Since the manganites show some tendency to phase separation,[12] a fundamental ambiguity arises in the study of strained thin films: is the insulating state an intrinsic property of the strained film or does it arise from extrinsic factors such as phase separation due to an inhomogeneous strain state? This question has not been fully clarified and studies supporting both scenarios can be found in the literature. Biswas *et al.*[6] argue that very thin insulating films deposited on $LaAlO_3$ under compressive stress have inherent two-phase character due to strain variations across growth islands. Similarly it was argued that $La_{0.7}Ca_{0.3}MnO_3$ films on $SrTiO_3$ show signs of phase separation near the interface.[8,13] Using high-resolution electron microscopy Zandbergen *et al.*[4] and Arita *et al.*[14] found a structure change in $La_{0.7}Ca_{0.3}MnO_3$ films on $SrTiO_3$ with a Jahn-Teller-like distortion due to the film-substrate misfit accompanied by a deformation of the basal oxygen square and extensive twinning. Klein *et al.*[10,11] studied $La_{0.7}Ca_{0.3}MnO_3$ films grown on $La_{0.7}Ba_{0.3}MnO_3$ and observed a large resistivity anisotropy that was explained within a model of orbital ordering.

The situation is likely to be even more complex. Apart from the presence of strain-induced phase separation in thin films there might be an intrinsic tendency to phase separation near the first-order transition between the ferromagnetic and antiferromagnetic (orbitally ordered) states.[12] Since the antiferromagnetic, orbitally ordered phase can be driven towards a ferromagnetic phase by the application of a magnetic field, large hysteretic effects in the magnetic and magnetotransport properties of thin films might be anticipated from the experience with single crystals.[1]

In this work the microstructural, magnetic, and magnetotransport properties of $La_{0.7}Ca_{0.3}MnO_3$ (LCMO) films epitaxially grown on $SrTiO_3$ were investigated as a function of film thickness. The films were fabricated using pulsed laser deposition (PLD) under identical conditions. This resulted in a series of films with varying strain states from relaxed film growth at large thickness (above about 70 nm) to coherently strained films below about 10 nm. The very thin films show magnetotransport properties very similar to those of charge-ordered bulk samples. From the analysis of the microstructure we were able to show that this behavior does not arise from strain variations across growth islands.

II. EXPERIMENTAL DETAILS

LCMO films were fabricated using PLD from a stoichiometric polycrystalline target onto (001) single-crystal $SrTiO_3$ substrates. Substrate temperature was 700 °C and oxygen partial pressure during deposition was 0.13 mbar. An Exci-

TABLE I. Parameters of the $La_{0.7}Ca_{0.3}MnO_3$ films on $SrTiO_3$ (001) investigated in this work. d denotes the film thickness, $a_\parallel$ and $a_\perp$ the in-plane and out-of-plane lattice parameter, respectively, and FWHM the full width at half maximum of the (002) reflection in a Θ-2Θ scan. The FWHM of the (002) substrate reflection was 0.02°. s_q is the mean-square roughness. The Curie temperature T_C was determined from the upper inflection point of the magnetization measured in a field of 0.1 T applied parallel to the film and by extrapolation of the coercive field to zero (value in brackets). In the case of sample LCSTO3 the coercive field was not measured; sample LCSTO5 had such a broad magnetization transition that an inflection point could not be sensibly defined.

Label	d (nm)	$a_\parallel$ (nm)	$a_\perp$ (nm)	FWHM (°)	s_q (nm)	T_C (K)
LCSTO1	280	0.3875	0.3833	0.37	2.6	273 (274)
LCSTO2	100	0.3877	0.3833	0.48	1.0	269 (272)
LCSTO3	70	0.3875	0.3833	0.34	0.9	263 (—)
LCSTO4	22	0.3905	0.3811	0.48	1.6	254 (260)
LCSTO5	9	0.3905	0.3810	1.18	2.4	—(220)

mer laser (Lambda Physik) operating at 308 nm (XeCl) with a pulse energy of 200 mJ was employed at a repetition rate of 10 Hz. The fluence on the target was estimated to be about 1 J/cm^2. After deposition the films were slowly cooled (cooling rate of approximately 4 K/min) to room temperature in an oxygen atmosphere of 0.13 mbar. Afterwards the films were transferred to a furnace and annealed for 2 h at 950 °C in 1 bar of flowing oxygen. The heating rate was about 8 K/min and cooling rate about 4 K/min. Film thickness was estimated from deposition time and has an uncertainty of about 10%.

In this work five LCMO films on $SrTiO_3$ were investigated. Some parameters of the films can be found in Table I.

X-ray diffractometry was used to characterize the films by recording detailed reciprocal space maps of the (002) and the (013) reflections with Cu K_{α_1} radiation in a high-resolution diffractometer. Surface topography was investigated by atomic force microscopy (AFM). The AFM measurements were performed using a Nanoscope IIIa with a Dimension 3000 scanning probe microscope (Digital Instruments) with an extender electronics module. The images were analyzed with the "scanning probe image processor (SPIP)" software. Root-mean-square roughness was calculated from images taken at four to six different positions on the film. In case of all films the variation of both roughness and microstructure across the film was insignificant.

Resistivity measurements were performed in an Oxford variable-temperature cryostat system equipped with a 9-T superconducting solenoid. A standard four-point method in van der Pauw configuration[15] was used. A constant current was supplied by a Keithley model 224 current source and the voltage was measured with a Keithley nanovoltmeter model 182. Contacts were made with silver paste. The current direction could be rotated by 90° by interchanging a voltage and a current lead. Although the contact configuration is not ideal from the viewpoint of having a well-defined angle between current direction and magnetic field, a comparison with four in-line contacts showed that the deviations were negligible. Thus on average the current direction can be reasonably well defined. The van der Pauw configuration was used, since it allows rotations of the current direction entirely by manipulations of the cables outside the cryostat without the necessity of making new contacts. Measurements to accurately determine the temperature dependence of the resistivity were performed at a very low temperature sweep rate of about 0.1 K/min. The magnetic field was always applied parallel to the film surface.

Magnetoresistance was calculated according to the pessimistic definition

$$\frac{\Delta\rho}{\rho_0}=\frac{\rho-\rho_0}{\rho_0}, \tag{1}$$

with ρ_0 being the resistivity in zero field.

Magnetization measurements were performed with a superconducting quantum interference device (SQUID) magnetometer (MPMS-7, Quantum Design). The diamagnetic contributions from the substrate and sample holder were measured above the Curie temperature and were subtracted from the data. All magnetization measurements were performed in magnetic fields applied parallel to the film.

III. EXPERIMENTAL RESULTS

A. Structural characterization

Θ-2Θ scans of the samples show only $(00L)$ reflections of the substrate and the film indicating the excellent texture of the film. The reflections could be indexed assuming cubic or tetragonal symmetry; the Miller indices (hkl) in this study are based on the pseudocubic cell.

The in-plane and out-of-plane lattice constants were determined from reciprocal space mappings of the (002) and (013) reflections, respectively. Films with thickness above 70 nm are partially relaxed, thinner films are—within the error bars—fully strained. Since x-ray diffractometry averages over the film thickness, strain relaxation throughout the thickness cannot be ruled out. The lattice constants are shown in Fig. 1(a) as a function of film thickness. In Fig. 1(b) the values for FWHM(2Θ) are presented. Whereas values around 0.4° are found for thicker films, the thinnest film has a significantly enhanced value of 1.2°; this indicates large strains within this film.

AFM images of the films show a grainy microstructure. As a function of film thickness there appears to be a change in morphology; this is illustrated in Fig. 2 showing AFM images of three films with thickness of 9 nm, 22 nm, and 100 nm, respectively. Both height and phase image are shown; the scan range was 1 μm by 1 μm. The films with thicknesses of 70 nm and above show an island structure. Samples LCSTO2 and LCSTO3 are quite smooth with root-mean-square roughness s_q of about 1 nm; LCSTO1 shows some roughening with $s_q = 2.6$ nm which is probably due to the large thickness. Note that the ratio s_q/d is approximately constant in this thickness range; see Fig. 1(c). The thinner films show a mazelike structure and especially the thinnest film, LCSTO5, consists of square-shaped terraces which can

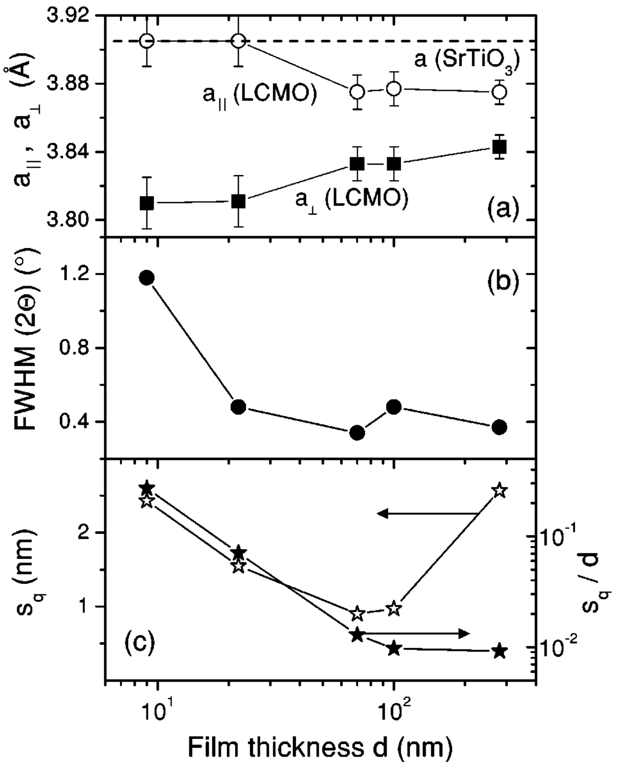

FIG. 1. (a) In- and out-of-plane lattice constants as determined from an analysis of the (002) and (013) reflections as a function of film thickness. The dashed line indicates the substrate lattice constant of SrTiO$_3$. Very thin films on SrTiO$_3$ adapt in-plane lattice constants equal to the substrate lattice constant. (b) Full width at half maximum FWHM(2Θ) of the (002) reflection. (c) Root-mean-square roughness as a function of film thickness (left axis). Dimensionless ratio s_q/d as a function of film thickness (right axis).

be clearly seen in the phase image. These terraces have an average height of 4 nm—i.e., about ten lattice constants. This film has a large ratio $s_q/d=0.27$. On the other hand, the AFM data clearly show that this film covers the substrate continuously.

High-resolution transmission electron microscopy (HRTEM) studies of various manganite thin films showed that the films grow coherently strained up to some critical thickness t_c.[16–19] Above this critical thickness misfit dislocations are nucleated in order to relieve the elastic strain. This is corroborated by x-ray investigations showing coherently strained growth up to t_c.[8–11,20] The value of the critical thickness varies according to deposition conditions, but might be as large as 100 nm[20] or even 180 nm.[9] Annealing leads to some strain relaxation—i.e., decreases t_c.[21] Lu *et al.*[22] found the nucleation of secondary phase rods in LCMO films on SrTiO$_3$ using HRTEM imaging and electron energy loss spectroscopy. These rods start at the interface and extend through the whole film thickness. Some of them are Ti enriched due to some interface reaction between film and substrate and subsequent diffusion. The x-ray diffractometry results presented here show that the strain state of the films changes as a function of thickness in agreement with literature data.[21,23–27] We believe from our results—in particular from the gradual evolution of the physical properties as a function of film thickness—and from literature data that the strain state essentially determines the transport and magnetic properties. We cannot definitely rule out an influence of secondary phases on the physical properties of the films; it seems unlikely, however, that these would determine the thickness variation of these properties, since the secondary phase rods have been shown to extend through the entire film thickness.[22]

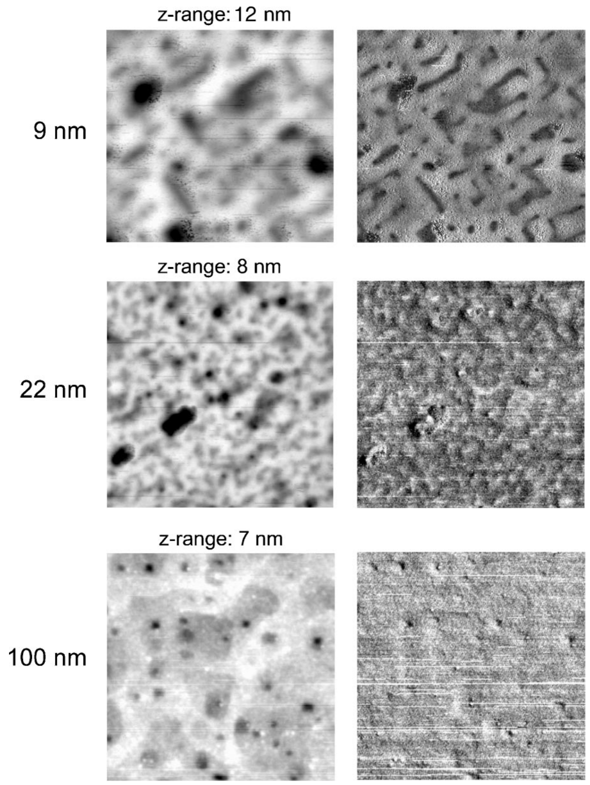

FIG. 2. AFM images of three LCMO films on SrTiO$_3$ recorded in contact mode. Both height (left column) and phase (right column) image are shown. The image size is 1×1 μm^2. Nominal film thickness and z range are indicated.

Coherently strained films might develop a morphological instability and show a rough surface with island growth.[28] We interpret the large surface roughness of the thinnest film as arising from island growth of a fully strained, but mainly dislocation-free film. The inhomogeneous strains around the islands will be estimated here from a simple model.[29] Ling[30] calculated the stress profile around a mound on a flat plate subjected to a uniform tension; see Fig. 3. Although this is only a two-dimensional model, it should be sufficient to derive semiquantitative estimates for the strain distribution in the films considered here.

Bipolar coordinates (ξ,η) are defined by

$$x+\mathrm{i}y=-R\coth\left[\frac{1}{2}\mathrm{i}(\xi+\mathrm{i}\eta)\right] \tag{2}$$

or equivalently

$$x=R\frac{\sinh(\eta)}{\cosh(\eta)-\cos(\xi)}, \tag{3a}$$

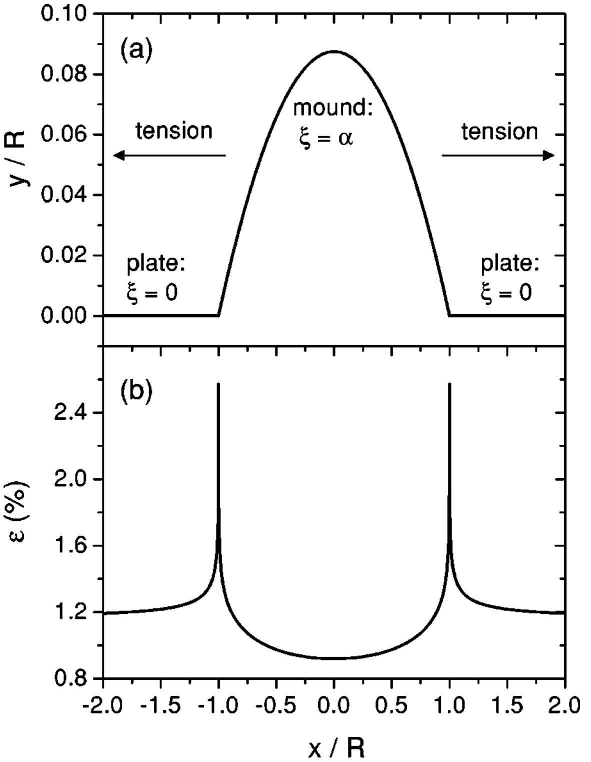

FIG. 3. (a) Cross section of Ling's mound. Rim of mound and plate are indicated. (b) Strain distribution across Ling's mound. For both calculations an angle $\beta = 5°$ was used.

$$y = -R\frac{\sin(\xi)}{\cosh(\eta) - \cos(\xi)}. \tag{3b}$$

R is the radius of the mound [see Fig. 3(a)], $-\infty < \eta < \infty$, and $0 \leqslant \xi \leqslant \alpha$. Here $\xi = \alpha$ is the rim of the mound, $\xi = 0$ the rim of the plate as indicated in Fig. 3(a). Let $h = y(\eta = 0, \xi = \alpha)$ denote the height of the mound; then $\tan(\beta) = h/R$ and $\alpha = \pi + 2\beta$. The shape of the mound is given by

$$x = R\frac{\sinh(\eta)}{\cosh(\eta) + \cos(2\beta)}, \tag{4a}$$

$$y = R\frac{\sin(2\beta)}{\cosh(\eta) + \cos(2\beta)}. \tag{4b}$$

The strain distribution was derived by Ling;[30] along the rim of the mound and the plate it is given by

$$\frac{\epsilon_{\eta\eta}}{\epsilon} = 2[\cosh(\eta) - \cos(\alpha)] \times \int_0^\infty \frac{n[n\cosh(n\alpha)\sin(\alpha) - \sinh(n\alpha)\cos(\alpha)]}{\sinh^2(n\alpha) - n^2\sin^2(\alpha)} \times \cos(n\eta)dn \quad \text{(mound)}, \tag{5a}$$

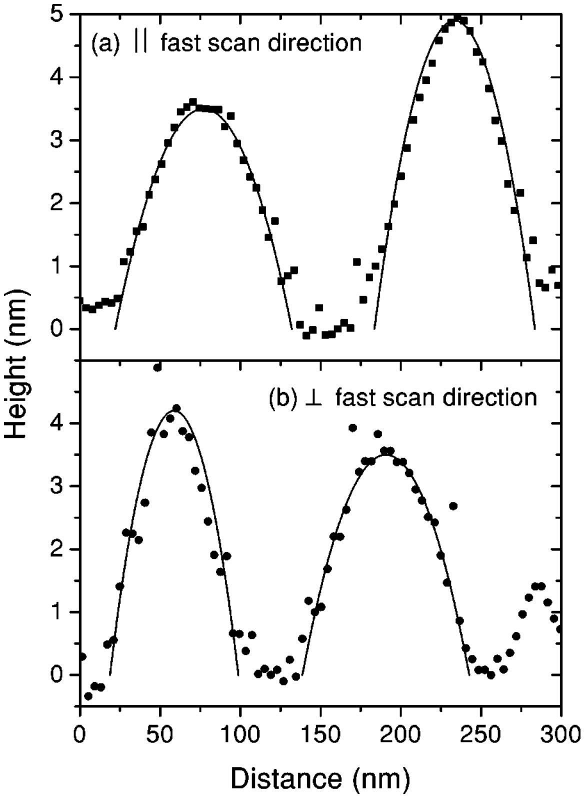

FIG. 4. Cross sections taken from the AFM image of sample LCSTO5 along (a) the fast and (b) the slow scan direction. The solid lines are fits of Ling's mound to the experimental height profiles.

$$\frac{\epsilon_{\eta\eta}}{\epsilon} = 1 + 2[\cosh(\eta) - 1] \times \int_0^\infty n\left[\coth(n\pi) - \frac{1}{2}\frac{\sinh(2n\alpha) - n\sin(2\alpha)}{\sinh^2(n\alpha) - n^2\sin^2(\alpha)}\right] \times \cos(n\eta)dn \quad \text{(plate)}. \tag{5b}$$

ϵ denotes the strain imposed by the film-substrate mismatch.

From the AFM images of sample LCSTO5 various cross sections parallel and perpendicular to the fast scan direction were extracted. These show a quite regular height variation such as shown in Fig. 4. The height profile was fitted with Eqs. (4a) and (4b) and values for the radius $R = 50 \pm 15$ nm and the characteristic angle $\beta = 5 \pm 1.5°$ were determined. With these values the strain distribution across the height profiles was calculated from Eqs. (5a) and (5b) by numerical integration; the result is shown in Fig. 3(b). The strain arising from the film-lattice mismatch is $\epsilon = (a_{STO} - a_{LCMO})/a_{LCMO} = 1.2\%$ with $a_{LCMO} = 0.386$ nm and $a_{STO} = 0.3905$ nm. The resulting strain profile is strongly peaked at the rim of the mound; near the crown of the mound it is reduced to about 78% of the strain imposed by the substrate.

B. Magnetization, resistivity, and magnetoresistance: General trends

In this section we discuss general trends seen in the magnetic and magnetotransport properties of the films. It will be

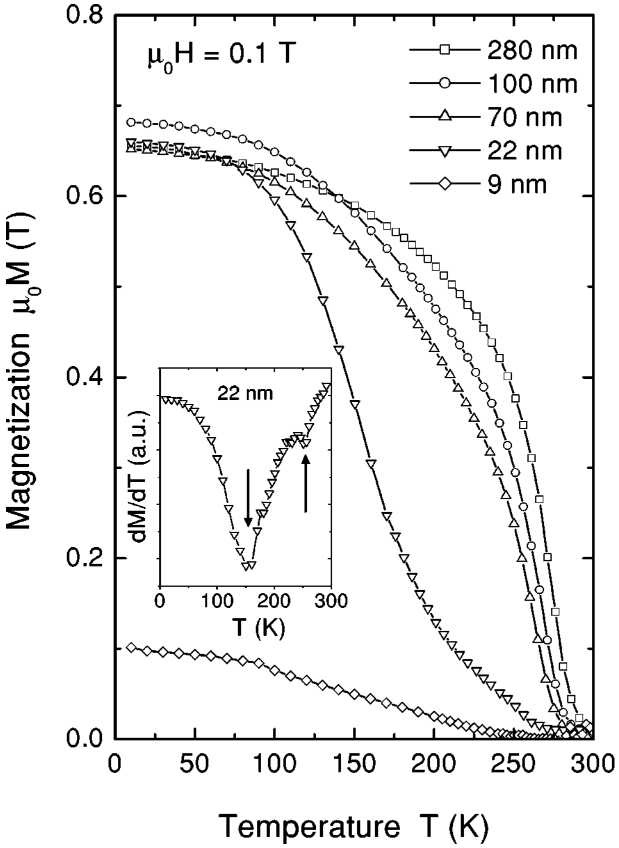

FIG. 5. Magnetization measured in an applied field of 0.1 T for the LCMO films with thicknesses between 9 and 280 nm. The inset shows dM/dT for sample LCSTO4.

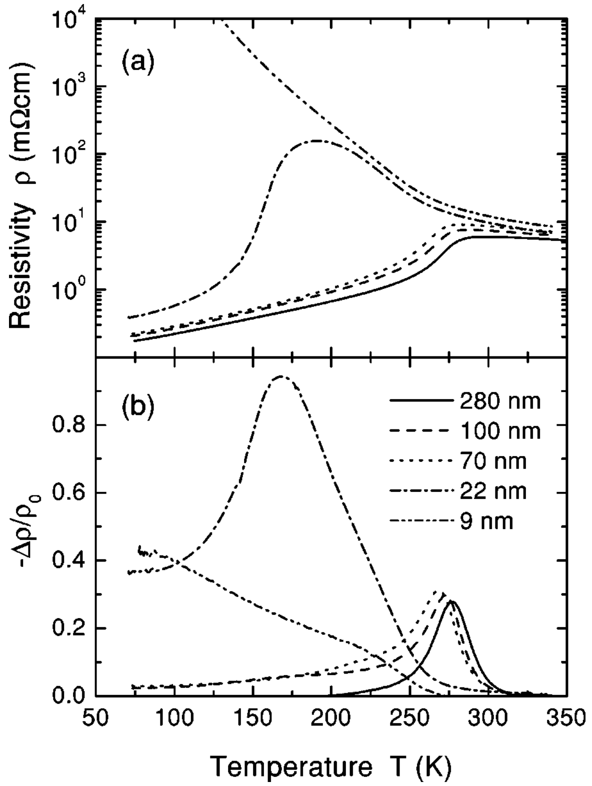

FIG. 6. (a) Zero-field resistivity and (b) magnetoresistance in an applied field of 1 T of LCMO films on $SrTiO_3$.

seen that the thickness dependence of these characteristics is significantly different compared to films grown on $LaAlO_3$.[31] From the structural characterization one would expect that films with thickness above 70 nm that have island structure and relaxed growth show bulklike magnetic and transport properties. This is indeed found in the magnetization and resistivity measurements. Figure 5 shows the magnetization measured in an applied field of 0.1 T during field cooled warming. Whereas thicker films with $d \geqslant 70$ nm show a sharp ferromagnetic transition with a Curie temperature above 260 K, the thinner films have a considerable magnetization tail with the magnetization being linear in temperature on approach of the Curie temperature. Except for sample LCSTO5 the films show a low-temperature magnetization value of about 0.65 T. This is smaller than the value of 0.74 T expected from the spin-only moment of $3.7\mu_B$. However, in an applied field of 0.1 T the magnetization is not fully saturated; the measured moment at low temperature approaches the spin-only moment in magnetic fields above 1 T. In the case of the thick films the Curie temperature can be readily defined by the inflection point of the magnetization, yielding the values given in Table I. Sample LCSTO4 shows two minima in dM/dT; see inset to Fig. 5. We identify the upper minimum as an indication of a bulklike Curie temperature; the corresponding value is listed in Table I. The lower minimum at 154 K corresponds to the rapid magnetization rise. The magnetization indicates the presence of two different strain states in the film: a quasirelaxed phase with a bulklike Curie temperature and a strained phase with a strongly reduced transition temperature. The magnetization variation of sample LCSTO5 with temperature is too gradual to enable a reliable determination of the Curie temperature.

The substrate imposes a biaxial strain $\epsilon^* = (2\epsilon_{zz} - \epsilon_{xx} - \epsilon_{yy})/2 = (a_\perp - a_\parallel)/(2a_{substrate})$ on the film. In cubic symmetry this leads to a decrease of the Curie temperature according to $T_c(\epsilon^*) = T_c(0)[1 - \delta_2(\epsilon^*)^2]$. Analysis of the data here yields $T_c(0) = 275.3$ K and $\delta_2 = 960$. This value is close to the value derived by Millis *et al.*[32] and indicates the significant influence of Jahn-Teller distortions.

The zero-field resistivity and magnetoresistance shown in Figs. 6(a) and 6(b), respectively, are in agreement with the magnetization behavior. Thick films have low residual resistivities of the order of 200 $\mu\Omega$ cm that slightly increase with decreasing film thickness. These films show a bulklike metal-insulator transition with a peaked magnetoresistance close to the Curie temperature. The metal-insulator transition of sample LCSTO4 corresponds to the lower magnetization transition; the thinnest film is insulating. Apparently, the 9-nm film is more severely strained than the 22-nm film, although the x-ray characterization yielded in-plane lattice constants equal to that of the $SrTiO_3$ substrate in both cases; we attribute this to the limited resolution of the x-ray diffractometer especially in case of very thin samples.

For a further characterization of the magnetic properties the coercive fields B_c were determined from magnetoresistance hysteresis loops recorded at various temperatures. It is well known[31,33] that maxima (minima) in the longitudinal

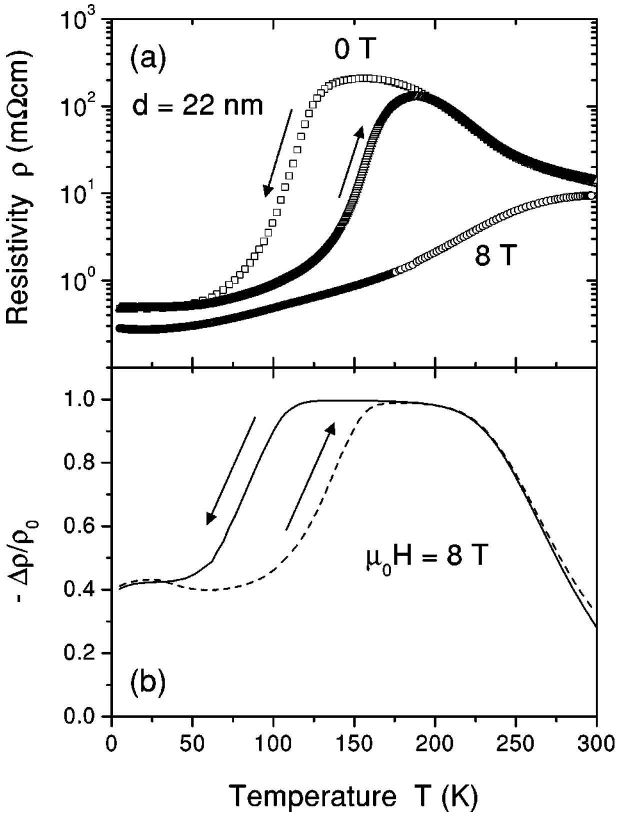

FIG. 7. (a) Resistivity and (b) magnetoresistance of sample LCSTO4, $d = 22$ nm, in an applied field of 8 T. The zero-field resistivity was measured on cooling and warming as indicated by the arrows.

(transverse) magnetoresistance appear at the coercive fields. The Curie temperature of the films was determined as the temperature of vanishing coercivity. The values obtained are listed in Table I and are in good agreement with the values derived from the magnetization measurements.

It was shown before[31] that the conductance G versus thickness at 77 K extrapolates to $G = 0$ at a finite thickness of 28.5 ± 5.4 nm. This is in agreement with the significant deviations from bulk behavior observed for the thinnest films.

From this rough characterization it is evident that the strain state and microstructure have a significant influence on the magnetic and transport properties. In the following sections the films will be further characterized in detail; we will especially concentrate on the strained films.

C. Intermediate thickness regime: Metallic hysteretic properties

Figure 7 shows the resistivity and magnetoresistance in an applied field of 8 T of sample LCSTO4 with a thickness of 22 nm. The most striking result is the appearance of a large hysteresis in the zero-field resistivity with respect to the cooling and heating cycles. This hysteresis which is absent in the resistivity measured in 8 T indicates a first-order transition in this strained LCMO film. The magnetoresistance has a broad plateau with a value of nearly 100%. The magnetization of this film as measured in various applied fields is presented in Fig. 8. At low temperatures there is a strong dependence on magnetic field with a saturation above 1 T at a magnetization value that closely corresponds to the spin-only value.

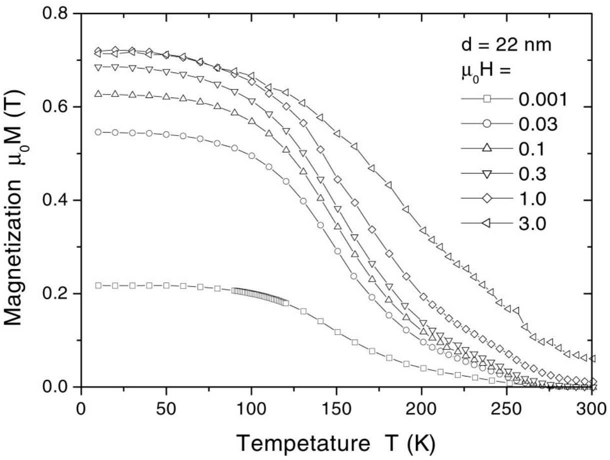

FIG. 8. Magnetization of sample LCSTO4 measured in various magnetic fields.

D. Ultrathin films: First-order metal-insulator transition

In this section magnetization and magnetotransport data of sample LCSTO5 with a thickness of 9 nm are discussed. This sample is of special interest, since it shows a strain-induced strongly hysteretic metal-insulator transition. The resistivity of this sample is shown in Fig. 9: in zero field the resistivity is insulating and below 100 K the resistance is too large to be measurable with our setup. If a magnetic field of 8 T is applied after zero-field cooling, a metal-insulator transition is seen and on warming the sample is metallic (○ in Fig. 9). Metallic behavior is also found on cooling from 300 K (× in Fig. 9). Below 50 K a hysteresis appears between the field-cooled and the zero-field-cooled curves. This indicates that below 50 K a field of 8 T is not sufficient to induce a fully metallic state after zero-field cooling.

Figure 10 shows resistivity hysteresis loops obtained after zero-field cooling to the measuring temperature. Below 100 K the resistance is too high to be measured after zero-field cooling. On the application of a magnetic field a sudden transition to a metallic state occurs. This metallic state is metastable and at 10 K and 60 K persists even down to zero field. It can be destroyed by heating to about 100 K. Note that there is strong hysteresis above the metal-insulator transition. This hysteresis is responsible for the thermal hysteresis observed in Fig. 9. At 100 K both transitions from the insulating to the metallic and from the metallic to the insulating state are seen. At 200 K the magnetoresistance is nearly reversible. We define the metal-insulator transition by the extrema in the resistivity derivative as a function of magnetic field. The phase diagram constructed in this way is shown in Fig. 11. The metallic and insulating phases are separated by a broad hysteretic region. Note the similarity of this phase diagram to the phase diagram of charge-ordered compounds of the type $Nd_{0.5}Sr_{0.5}MnO_3$.[1]

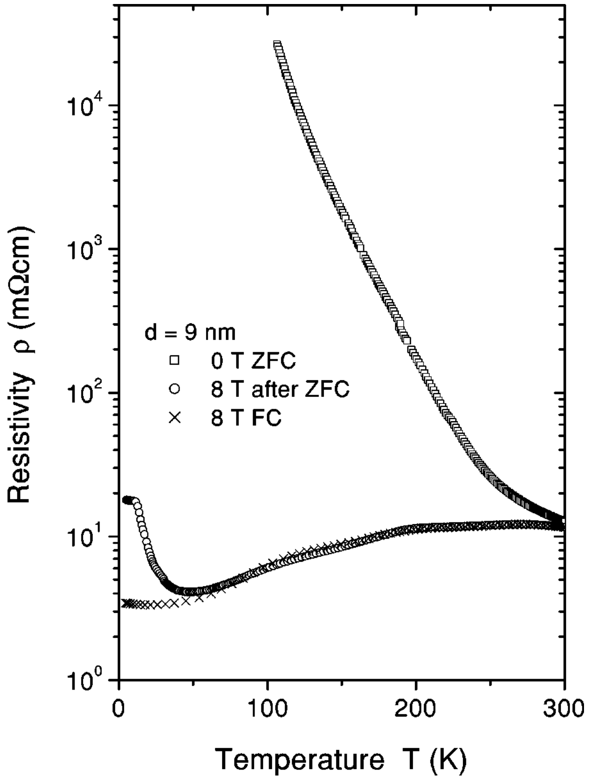

FIG. 9. Resistivity of sample LCSTO5 (9 nm) in zero field, in a field of 8 T applied after zero field cooling, and during field cooling (FC) in 8 T. The current is parallel to the applied field.

The metallic state was found to be inhomogeneous. This is shown in Fig. 12: here a metallic state was induced after zero-field cooling to 10 K by the application of a field of 8 T. If the current is parallel to the magnetic field [see Fig. 12(a)] a resistance of 4545 Ω is obtained. On the other hand, if the current is perpendicular to the magnetic field [see Fig. 12(b)] the apparent resistance is only 10 Ω and below 1.5 μA there is a significant negative voltage offset. Moreover, the signal is very noisy and indicates the presence of many fluctuators. As discussed in Sec. II the measurements were performed in the van der Pauw configuration and the current is not exactly parallel to the magnetic field. Therefore, we interpret the signal for the transverse configuration as arising from a current meandering along metallic stripes which are mainly parallel to the magnetic field; the voltage from these current paths is added nearly to zero as observed experimentally. We conclude that the sample consists of alternating metallic and insulating stripes as indicated in the inset of Fig. 12.

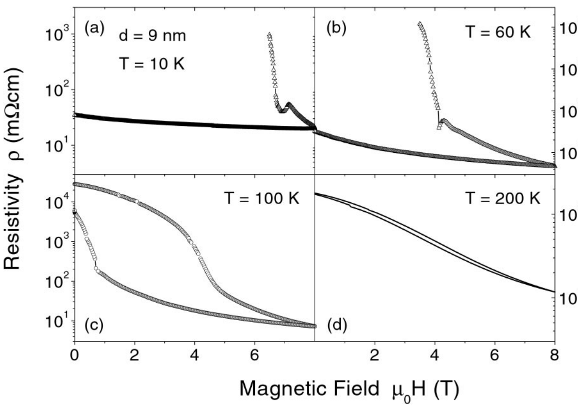

FIG. 10. Resistivity hysteresis loops measured after zero-field cooling to the indicated temperature.

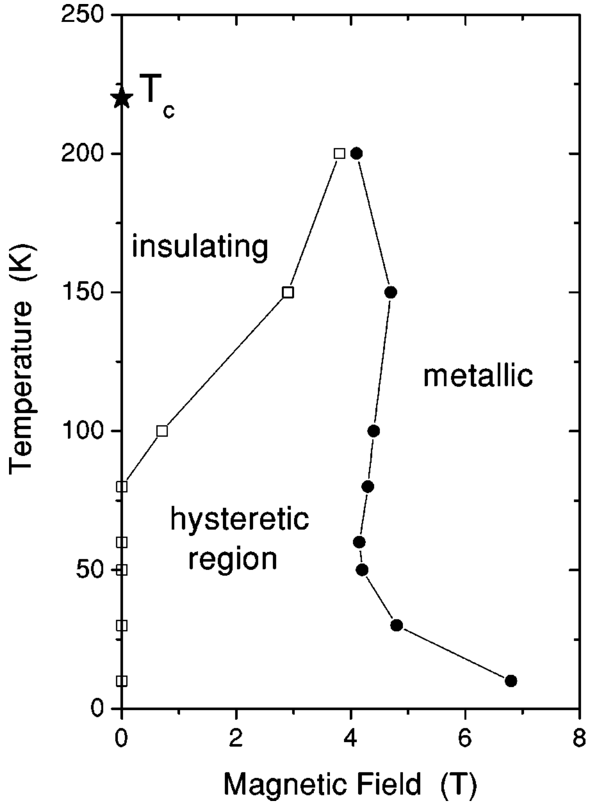

FIG. 11. Phase diagram of sample LCSTO5 as obtained from the magnetotransport measurements.

The resistivity irreversibility is also reflected in the magnetization. A magnetization hysteresis loop at 30 K obtained after zero-field cooling is shown in Fig. 13(a). The virgin curve shows a strong ferromagnetic rise to a magnetization M_v followed by a linear increase which does not saturate up to the maximum field of 7 T. The consecutive hysteresis loop from 7 T to -7 T to 7 T is reversible—apart from domain effects in magnetic fields of the order of the coercive field. The remanence M_{rem} is considerably higher than the initial ferromagnetic magnetization M_v; i.e., the magnetic field induces a significant ferromagnetic magnetization contribution $M_{ind}=M_{rem}-M_v$. Values of M_{rem}, M_v, and the induced magnetization fraction

$$p_{ind}=\frac{M_{rem}-M_v}{M_{rem}} \tag{6}$$

are shown in Fig. 13(b). p_{ind} decays with temperature from a rather high value of 0.7 at 10 K to zero at about 200 K in agreement with the vanishing of the magnetoresistance hysteresis above that temperature. The magnetization of sample LCSTO5 does not reach the spin-only value of 0.7 T. Within

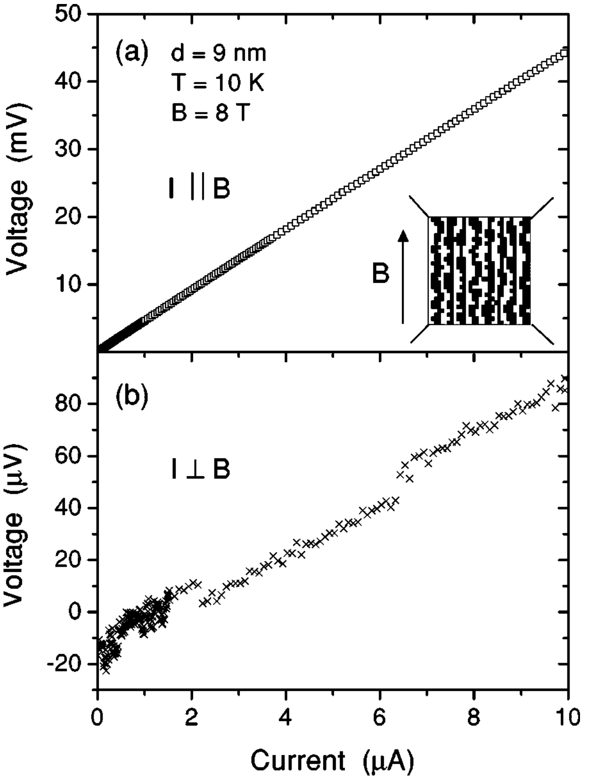

FIG. 12. Voltage-current characteristics of sample LCSTO5 obtained at 10 K in a magnetic field of 8 T for currents applied (a) longitudinal and (b) transverse to the magnetic field. The field was applied after zero-field cooling to 10 K. The inset shows a configuration of the sample with alternating metallic and insulating stripes parallel to the field direction. The current and voltage leads are indicated as lines at the four edges.

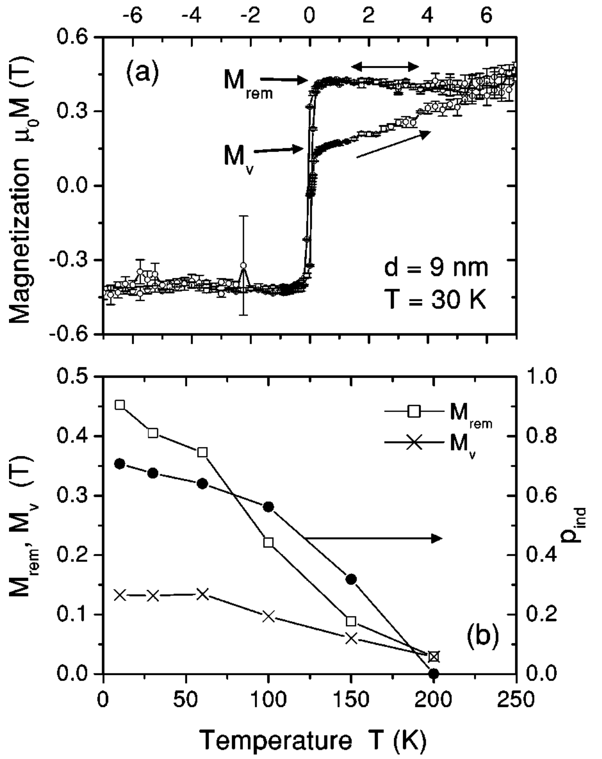

FIG. 13. (a) Magnetization hysteresis loop obtained at 30 K after zero-field cooling. Virgin curves and subsequent (reversible) hysteresis loop are indicated by the arrows. The remanent magnetization M_{rem} and the initial ferromagnetic contribution M_v are indicated by arrows. (b) Remanent magnetization M_{rem}, initial ferromagnetic magnetization M_v of the virgin curve, and fraction of induced magnetization, p_{ind}, as a function of temperature.

the resolution of the measurement, however, the high-field magnetization slope of the hysteresis loop is zero after having reached 7 T once.

By analogy with the general behavior of manganites at half filling[1] one might conclude from the magnetotransport data presented here that sample LCSTO5 shows orbital ordering. The orbital order is destroyed by the application of a large magnetic field and a metastable ferromagnetic metallic state is induced. As judged from the large hysteresis, the transition is undoubtedly of first order. The magnetization data indicate that the insulating, orbitally ordered state is ferromagnetic with a reduced saturation moment. We cannot firmly conclude that this ferromagnetism is intrinsic to the orbitally ordered state or that it arises from variations of the strain state or sample thickness over the sample area—i.e., on length scales of the order of 1 mm. AFM data recorded at five locations on the sample indicate the same morphology at these positions, but the area scanned in these investigations is small compared to the sample area of 5×5 mm^2.

The insulating state of the strained thin LCMO film can be understood as arising from the induced tetragonal distortion. First we consider a homogeneous strain distribution. From x-ray diffractometry, in the thinnest film an axis ratio $c/a \simeq 0.976$ is realized. The tensile strain arising from the film-substrate lattice mismatch is $\epsilon \simeq 1.2\%$. The tetragonal distortion has two effects.[2] First, the degeneracy of the e_g orbitals is lifted such that the $3z^2-r^2$ orbitals oriented along the c axis will be less populated than the x^2-y^2 ones in the basal plane. This weakens the double-exchange interaction along the c axis, whereas it is enhanced within the basal plane which, in turn, favors *A*-type antiferromagnetic ordering. A second effect is due to the bandwidth dependence of the ferromagnetic double-exchange and antiferromagnetic superexchange interactions. If the Mn-Mn distance is decreased (increased), the bandwidth increases (decreases). The band structure is such that the nearest-neighbor exchange interaction is weakened along the contracted bond—i.e., the substrate normal. This mechanism also favors *A*-type antiferromagnetic ordering.

Using band-structure calculations Fang *et al.*[2] determined the phase diagram of tetragonal manganites as a function of doping and tetragonal distortion. The calculations were performed for $La_{0.7}Sr_{0.3}MnO_3$ (LSMO). At a doping $x=0.3$ the transition from a ferromagnetic metallic state to an *A*-type antiferromagnetic insulating state occurs at an axis ratio $c/a \simeq 0.96$. This is clearly smaller than the experimental value assuming a homogeneous strain distribution. However, if the calculation is performed for LSMO with a hypothetical unit cell volume expanded by 9% with respect to the experimental one, the phase-diagram region occupied by the ferromagnetic metallic state expands. This indicates that in case of LCMO with a smaller unit cell volume than LSMO, the transition should occur at a larger c/a ratio in agreement with experiment. Moreover, the transitions between the ferromagnetic and antiferromagnetic phases are supposed to be of first order, which was not taken into account in the calculation. We conclude that in the case of LCMO an axis ratio $c/a \simeq 0.976$ might be sufficient to induce an orbitally ordered insulating phase.

Biswas *et al.*[5,6] argued that the insulating state observed in thin LCMO films on $LaAlO_3$ might arise from an inhomogeneous strain distribution across growth islands: the center of the grains is ferromagnetic metallic, whereas the highly strained rim is insulating and nonferromagnetic. In case of sample LCSTO5 the situation is radically different. The quantitative analysis of the strain distribution across grain profiles as shown in Figs. 3 and 4 gives evidence that the strain variation across the grain profile is quite small. This strain variation induces a variation of the c/a ratio that is strongly peaked at the grain boundary such that the sample fraction with a strongly reduced c/a ratio below 0.97 is very small. On the other hand, the magnetization data presented in Fig. 13(b) show that the fraction of induced metallic phase reaches 70% at low temperatures. This means that the antiferromagnetic phase is not restricted to thin regions near the grain edges, but occupies a substantial part of the film. Therefore, the induced insulating state must have a quite homogeneous strain distribution. We conclude that the metal-insulator transitions observed in sample LCSTO5 are not due to extrinsic phase separation induced by an inhomogeneous strain distribution, but are an intrinsic property of the strained film. This does not exclude, however, that this insulating phase has a tendency to an intrinsically driven phase segregation. In fact, measurements of I-V curves under applied magnetic field indicate the existence of conducting stripes along the magnetic field direction.

IV. DISCUSSION AND CONCLUSIONS

In this work the structural, magnetic, and magnetotransport properties of $La_{0.7}Ca_{0.3}MnO_3$ films deposited on $SrTiO_3$ were investigated as a function of thickness in the range between 9 and 280 nm. The strain state was found to change drastically from relaxed heteroepitaxial growth above about 70 nm to fully strained film growth at 9 nm thickness. We attribute changes in the magnetic and magnetotransport properties to this change of the strain state.

The magnetotransport properties of thick films are standard bulk like.[34] On decrease of the film thickness hysteresis develops in the zero-field resistivity curves measured on cooling and warming, respectively. This indicates that the continuous metal-insulator transition seen in thick films is driven towards a first-order transition in thinner films. A 9-nm-thick film is insulating, but ferromagnetic in zero field. The saturation magnetization, however, is reduced compared to the bulk value. In a large static magnetic field, this film shows a strongly hysteretic metal-insulator transition. The metastable metallic phase was found to be asymmetric with respect to the relative direction of the magnetic field and probing current. The magnetization in the field-induced metallic state is significantly larger than in the insulating state.

Similar insulating states have been observed in thin manganite films grown under tensile stress on $SrTiO_3$ (Refs. 3 and 4) and under compressive stress on $LaAlO_3$ (Refs. 3, 5, and 6). These have been interpreted as due to strain-driven phase separation into ferromagnetic metallic and antiferromagnetic insulating states[5,6] or as arising from bulklike orbital ordering.[3] By a quantitative analysis of the strain distribution across grain profiles of the thinnest film and a comparison with the magnetization data it could be shown here that the insulating state is not due to extrinsic strain-driven phase separation. It is an intrinsic property of coherently strained films as suggested by Konishi *et al.*[3] The metallic state—induced by the application of a large magnetic field—shows indications for a stripe phase which might be interpreted as an intrinsic tendency towards phase separation.

For $La_{0.7}Sr_{0.3}MnO_3$ Fang *et al.*[2] found a value $c/a \simeq 0.96$ for the tetragonal distortion at the transition from the ferromagnetic metallic to the insulating A-type antiferromagnetic phase. Assuming a homogeneous strain $\epsilon \simeq 1.2\%$ as determined from x-ray diffractometry, in the thinnest film $c/a \simeq 0.976$ is realized. This is considerably larger than the theoretical value. However, the calculations were performed for Sr doping with experimental volumes and a hypothetical expanded unit cell and this shows that the metallic state is more stable in the expanded lattice. Since the unit cell further contracts for Ca doping, this might lead to a larger theoretical c/a ratio at the transition. From the experimental evidence presented here we propose that the metal-insulator transition observed in coherently strained LCMO films on $SrTiO_3$ is due to orbital ordering in a homogeneous phase.

ACKNOWLEDGMENTS

This work was supported by the DFG under Contract No. DFG ES 86/7-1 within the Forschergruppe ‘‘Oxidische Grenzflächen’’ and under Contract No. DFG ES 86/6-1.

---

*Electronic address: ziese@physik.uni-leipzig.de

[1] Y. Tokura and N. Nagaosa, Science **288**, 462 (2000).

[2] Z. Fang, I.V. Solovyev, and K. Terakura, Phys. Rev. Lett. **84**, 3169 (2000).

[3] Y. Konishi, Z. Fang, M. Izumi, T. Manako, M. Kasai, H. Kuwahara, M. Kawasaki, K. Terakura, and Y. Tokura, J. Phys. Soc. Jpn. **68**, 3790 (1999).

[4] H.W. Zandbergen, S. Freisem, T. Nojima, and J. Aarts, Phys. Rev. B **60**, 10 259 (1999).

[5] A. Biswas, M. Rajeswari, R.C. Srivasta, T. Venkatesan, R.L. Greene, and A.J. Millis, Phys. Rev. B **61**, 9665 (2000).

[6] A. Biswas, M. Rajeswari, R.C. Srivasta, T. Venkatesan, R.L. Greene, Q. Lu, A.L. de Lozanne, and A.J. Millis, Phys. Rev. B **63**, 184424 (2001).

[7] P. Padhan, N.K. Pandey, S. Srivastava, R.K. Rakshit, V.N. Kulkarni, and R.C. Budhani, Solid State Commun. **117**, 27 (2001).

[8] M. Bibes, L. Balcells, S. Valencia, J. Fontcuberta, M. Wojcik, E.

Jedryka, and S. Nadolski, Phys. Rev. Lett. **87**, 067210 (2001).

[9] M. Bibes, M.-J. Casanove, L. Balcells, S. Valencia, B. Martínez, J.-C. Ousset, and J. Fontcuberta, Appl. Surf. Sci. **188**, 202 (2002).

[10] J. Klein, J.B. Philipp, G. Carbone, A. Vigilante, L. Alff, and R. Gross, Phys. Rev. B **66**, 052414 (2002).

[11] J. Klein, J.B. Philipp, D. Reisinger, M. Opel, A. Marx, A. Erb, L. Alff, and R. Gross, J. Appl. Phys. **93**, 7373 (2003).

[12] E. Dagotto, T. Hotta, and A. Moreo, Phys. Rep. **344**, 1 (2001).

[13] M.-H. Jo, N.D. Mathur, J.E. Evetts, M.G. Blamire, M. Bibes, and J. Fontcuberta, Appl. Phys. Lett. **75**, 3689 (1999).

[14] M. Arita, A. Sasaki, K. Hamada, A. Okada, J. Hayakawa, H. Asano, M. Matsui, and H. Takahashi, J. Magn. Magn. Mater. **211**, 84 (2000).

[15] L.J. van der Pauw, Philips Tech. Rev. **20**, 220 (1958).

[16] O.I. Lebedev, G.V. Tendeloo, S. Amelinckx, B. Leibold, and H.-U. Habermeier, Phys. Rev. B **58**, 8065 (1998).

[17] B. Wiedenhorst, C. Höfener, Y. Lu, J. Klein, L. Alff, B.H. Freitag, and W. Mader, Appl. Phys. Lett. **74**, 3636 (1999).

[18] G. van Tendeloo, O.I. Lebedev, and S. Amelinckx, J. Magn. Magn. Mater. **211**, 73 (2000).

[19] O.Y. Gorbenko, I.E. Graboy, A.R. Kaul, and H.W. Zandbergen, J. Magn. Magn. Mater. **211**, 97 (2000).

[20] M. Izumi, Y. Konishi, T. Nishihara, S. Hayashi, M. Shinohara, M. Kawasaki, and Y. Tokura, Appl. Phys. Lett. **73**, 2497 (1998).

[21] G.M. Gross, F.S. Razavi, R.B. Praus, and H.-U. Habermeier, J. Magn. Magn. Mater. **211**, 22 (2000).

[22] C.J. Lu, Z.L. Wang, C. Kwon, and Q.X. Jia, J. Appl. Phys. **88**, 4032 (2000).

[23] R.A. Rao, D. Lavric, T.K. Nath, C.B. Eom, L. Wu, and F. Tsui, Appl. Phys. Lett. **73**, 3294 (1998).

[24] A. Barman and G. Koren, Appl. Phys. Lett. **77**, 1674 (2000).

[25] W. Prellier, C. Simon, B. Mercey, M. Hervieu, A.M. Haghiri-Gosnet, D. Saurel, P. Lecoeur, and B. Raveau, J. Appl. Phys. **89**, 6612 (2001).

[26] J. Zhang, H. Tanaka, T. Kanki, J.-H. Choi, and T. Kawai, Phys. Rev. B **64**, 184404 (2001).

[27] K.-H. Müller, K. Dörr, T. Walter, M. Sahana, K. Brand, and L. Schultz, J. Magn. Magn. Mater. **242-245**, 447 (2002).

[28] B.J. Spencer, Phys. Rev. Lett. **67**, 3696 (1991).

[29] Y. Chen and J. Washburn, Phys. Rev. Lett. **77**, 4046 (1996).

[30] C.-B. Ling, J. Math. Phys. **26**, 284 (1948).

[31] M. Ziese, H.C. Semmelhack, K.H. Han, S.P. Sena, and H.J. Blythe, J. Appl. Phys. **91**, 9930 (2002).

[32] A.J. Millis, T. Darling, and A. Migliori, J. Appl. Phys. **83**, 1588 (1998).

[33] M. Ziese and S.P. Sena, J. Phys.: Condens. Matter **10**, 2727 (1998).

[34] J.M.D. Coey, M. Viret, and S. von Molnár, Adv. Phys. **48**, 167 (1999).